High Resolution fMRI using Compressed Sensing

by

Vasiliy Karasev

submitted in partial satisfaction
of the requirements for the degree of

Master of Science

in

Electrical Engineering

in the

GRADUATE DIVISION

of the

UNIVERSITY OF CALIFORNIA, LOS ANGELES

Committee in charge:

Professor Jin Hyung Lee

Spring 2011

Abstract

While functional magnetic resonance imaging (fMRI) is widely used in studies of brain functions, spatiotemporal resolution of the technique is limited. Conventionally, increasing spatial resolution requires acquiring more samples to satisfy Nyquist rate, leading to inadequately long scan time. When Nyquist sampling rate is violated, resulting image is degraded by aliasing artifacts. However, recent work in field of compressed sensing and previous applications of compressed sensing to MRI have demonstrated that images can be accurately reconstructed from fewer samples than necessary: scan times can be reduced without loss of image quality. This work describes an application of compressed sensing to fMRI, demonstrating accurate reconstruction of activation maps and blood level oxygenation dependent (BOLD) signal time series, from significantly undersampled data. We then show that the potential reduction in scan time can instead be traded off for substantially improved spatial resolution. Specifically, our method allows us to attain more than five-fold increase in image matrix size, with no loss of volume coverage, decrease in temporal resolution, or any changes to relevant imaging parameters. Results are shown on two optogenetic fMRI datasets.

Contents

1 Introduction 1

2 Background 2

3 Methods 4

4 Experiments 6

4.1 Phantom Experiment 7

4.2 Undersampled fMRI experiment 8

4.3 High Resolution fMRI 10

5 Discussion 12

Bibliography **17**

1 Introduction

Due to its non-invasive nature and availability, functional magnetic resonance imaging (fMRI) plays a dominant role in studies of brain functions. Most commonly used approach utilizes blood oxygenation level-dependent (BOLD) contrast[1] and measures deoxyhemoglobin concentration variations in regions of neuronal activity. Technique makes it possible to image activity in the entire brain when subject is presented a stimulus or performs a task.

Despite fMRI's wide use, technique has resolution limitations. Ability to discern subregions within activated areas requires high spatial resolution; however, this demands increasing scan time leading to inadequate temporal sampling of signal dynamics, or losing full brain coverage needed to study brain connectivity. Field of view, spatial, and temporal resolutions need to be traded off. These tradeoffs, as well as intrinsic constraints of the technique limit conclusions that can be drawn from fMRI data.

One source of these constraints is in magnetic resonance (MR) system hardware, which requires sequential sampling, leading to lengthy acquisitions, whose duration increases with spatial resolution or field-of-view. A significant amount of research work on MR systems is focused on reducing scan time by acquisition protocol optimization, hardware improvements, and post-processing steps. Because scan time is proportional to the number of acquired k-space samples, a simple way to reduce scan time is to decrease the number of sampled points, thus violating Nyquist sampling rate criteria. This leads to image degradation: aliasing artifacts or loss of spatial resolution. However, research in field of compressed sensing demonstrates that if one introduces weak restrictions on the underlying signal and the acquisition system, exact reconstruction is possible from highly incomplete information [2; 3]. For MR, this implies that images can be accurately reconstructed from fewer k-space samples than necessary by Nyquist rate: scan times can be significantly reduced without loss of image quality.

In this work, we describe an application of compressed sensing framework to fMRI. We demonstrate feasibility of significantly reducing the number of acquired k-space samples,

while preserving image quality, providing accurate activation maps, and precisely reconstructing BOLD time course. Performance of the method is examined on simulated phantom data and a real optogenetic fMRI[4] (ofMRI) dataset. We then show that the framework can be used to substantially improve spatial resolution in fMRI. Specifically, our method allows us to attain more than five-fold increase in encoding matrix size, with no loss of volume coverage, decrease in temporal resolution, or any changes to relevant imaging parameters. Results are shown on two ofMRI datasets.

2 Background

Reconstruction of MR images from acquired k-space data can be viewed as the problem of finding a solution to a system of linear equations. If k-space is undersampled, the problem is underdetermined. Let $x \in \mathbb{C}^n$ be an image, $y \in \mathbb{C}^m$ - measured k-space data, and $F \in \mathbb{C}^{m \times n}$ - the partial Fourier transform matrix. We seek the solution x, but since k-space is undersampled, $m \ll n$, F is "fat", and there are infinitely many solution vectors satisfying $y = Fx$. Typically, in these cases, it is common to choose x that satisfies the minimum energy property:

$$\text{minimize } ||x||_2 \text{ subject to } Fx = y \tag{1}$$

However, this leads to undesirable aliasing artifacts, which can be suppressed only if additional knowledge of the signal is available.

Recently, theoretical results in field of information theory demonstrated that exploiting prior knowledge of signal sparsity or compressibility makes it possible to exactly solve highly underdetermined problems. Let Ψ be a transform (e.g. wavelet, finite difference, discrete cosine) that provides means for describing signal of interest x with few significant terms. Then, if the acquisition matrix F and sparsifying transform Ψ are mutually incoherent [5],

reconstruction of x is possible by solving *Basis Pursuit* problem:

$$\text{minimize } ||\Psi x||_1 \text{ subject to } Fx = y \tag{2}$$

Sparsity of the solution in range of Ψ is enforced by ℓ_1 norm - a convex relaxation of combinatorial ℓ_0 semi-norm, while the constraint limits search over x to the subspace consistent with acquired data. Above formulation can be solved efficiently by interior point methods, but only when the size of the problem is small. In large scale situations, it is common to use first-order methods (gradient descent, nonlinear conjugate gradient) to solve an unconstrained problem:

$$\text{minimize } \frac{1}{2}||Fx - y||_2^2 + \lambda||\Psi x||_1 \tag{3}$$

Compressed sensing formulation is relevant for MR, since data acquisition occurs in alternate domain (k-space) and medical images are known to be compressible. In fact, a toy example suggesting use of optimization problem (2) in MR image reconstruction was early described in [2]. Since then, compressed sensing has been successfully applied in various MR settings. Lustig et al. give a thorough description of CS-MRI using multislice 2D-DFT brain imaging and 3D angiography as examples in [6]. Sparsity of these datasets is demonstrated under wavelet and total variation transforms. Ajraoui et al. demonstrate acceleration in ^{3}He lung imaging, using wavelets to compress images in [7]. Kim and Nayak reduce sampling time in 3D upper airway MRI, by enforcing data sparsity under total variation transform [8].

In dynamic MRI, where temporal redundancy of the data can be exploited, cardiac imaging received most attention, with several different proposed reconstruction schemes. Periodicity of cardiac cycles is used to sparsify temporal dimension of the data via Fourier transform in [9]. Gamper et al [10] propose a greedy reconstruction algorithm based on orthogonal matching pursuit. kt-FOCUSS, a reconstruction scheme inspired by video coding, which performs data compression using motion estimation and residual encoding stages, is

described in [11]. A method extending kt-FOCUSS to functional imaging is described by Jung and Ye in [12]. Aside from the last work, we are not aware of applications of compressed sensing to fMRI. This is surprising, since the imaging application can readily benefit from technological MR improvements, and it is by no means a niche field.

3 Methods

In a functional MRI experiment, a sequence of brain images is rapidly acquired over the course of several minutes. Signal of interest – variations in blood oxygenation – manifests itself as small changes in signal intensity in regions of neuronal activity. Ideally, acquisition proceeds without any subject motion, and the acquired image does not change significantly from frame to frame. Therefore, the captured dataset contains an enormous amount of redundancy and can be compressed *temporally*, as well as *spatially*. To exploit this, we require the reconstructed signal to be sparse under spatial and temporal finite difference transforms. Regularization by finite differences (also referred to as total variation) has been well known since [13], and is popular in image processing applications. In CS-MRI, it's been previously used in [6; 8; 14; 15].

Let us define some notation pertaining to our problem formulation. Suppose the fMRI experiment consists of T frames, and let $x^{(i)}$ represent image-domain data, $y^{(i)}$ – measured k-space data, and $F^{(i)}$ the partial Fourier matrix, all corresponding to i^{th} frame. Further, denote by $x = (x^{(1)}, x^{(2)}, ..., x^{(T)})$ the entire fMRI sequence in image domain, by $y = (y^{(1)}, y^{(2)}, ..., y^{(T)})$ – all k-space data acquired over the course of the experiment, and by $F = \text{diag}\{F^{(1)}, F^{(2)}, ..., F^{(T)}\}$ the collection of all Fourier matrices used in the experiment.

The underdetermined system of equations we are attempting to solve is then:

$$\begin{pmatrix} y^{(1)} \\ y^{(2)} \\ y^{(3)} \\ \vdots \\ y^{(T)} \end{pmatrix} = \begin{pmatrix} F^{(1)} & 0 & 0 & \dots & 0 \\ 0 & F^{(2)} & 0 & \dots & 0 \\ 0 & 0 & F^{(3)} & \dots & 0 \\ \vdots & \vdots & \vdots & \ddots & 0 \\ 0 & 0 & 0 & \dots & F^{(T)} \end{pmatrix} \begin{pmatrix} x^{(1)} \\ x^{(2)} \\ x^{(3)} \\ \vdots \\ x^{(T)} \end{pmatrix} \tag{4}$$

written compactly as $y = Fx$, as before. Let $D_1, ..., D_4$ be the difference operators along each of the four physical dimensions of the dataset. Specifically, if $m[i, j, k, l]$ is the 4-D representation of the image, with physical dimensions indexed by i, j, k, l, D_1 computes $\hat{m}[i, j, k, l] = m[i, j, k, l] - m[i-1, j, k, l]$, D_2 computes $\hat{m}[i, j, k, l] = m[i, j, k, l] - m[i, j-1, k, l]$, and so on. All operations satisfy circular boundary conditions. Denote by $\psi(.)$ the smooth approximation to the nondifferentiable ℓ_1 norm: $||x||_1 \approx \psi(x) = \sum_i (\sqrt{x_i^* x_i + \mu^2} - \mu)$. Then the problem is:

$$\text{minimize } \frac{1}{2}||Fx - y||_2^2 + \sum_{i=1}^{4} \lambda_i \psi(D_i x) \tag{5}$$

The regularization term $\sum_{i=1}^{4} \psi(D_i x)$ is essentially the anisotropic total variation penalty for 4-D datasets.

Gradient descent method with efficient backtracking line search is used to find the solution. Algorithm 1 below explicitly describes the procedure. Typical parameter values used in reconstructions were $\alpha = 5 \times 10^{-3}$, $\beta = 0.5$, $\lambda_1 = \lambda_2 = \lambda_3 = \lambda_4 = 10^{-4}$, $\mu = 10^{-4}$. Algorithm was terminated after maximum allowed number of iterations (typically 300-500) or after fractional change in function value reached small values: $|f(x^k) - f(x^{k-1})|/|f(x^k)| \leq 10^{-7}$. Fourier transforms are performed using a non-uniform FFT implementation by Fessler and Sutton [16] (modified to perform FFT calculations on a GPU), as it is extremely stable in iterative reconstructions. One reason gradient descent was chosen over more sophisticated algorithms is due to large size of the problem. As formulated, the entire fMRI sequence is a single optimization variable $x \in \mathbb{C}^n$. Especially in high resolution fMRI reconstructions, n

is very large: for some results shown in this report $n = 167 \times 167 \times 32 \times 130 = 116,018,240$. Storing several instances of these long vectors is prohibited by memory limits. But, due to its simplicity, gradient descent requires little memory, making it suitable for this application.

Algorithm 1 Gradient descent

Require: initial value of x, $\alpha \in (0, 0.5)$, $\beta \in (0, 1)$
Ensure: x minimizes $\frac{1}{2}||Fx - y||_2^2 + \sum_{i=1}^{4} \lambda_i \psi(D_i x)$
  repeat
    $\nabla f(x) \leftarrow F^H(Fx - y) + \sum_{i=1}^{4} \lambda_i D_i^T \nabla\psi(D_i x)$, where $\nabla\psi(x) = \frac{x}{\sqrt{x^* x + \mu^2}}$
    $t \leftarrow 1$
    $f_{lin} \leftarrow f(x) - \alpha t||\nabla f(x)||_2^2$
    $f_{new} \leftarrow f(x - t\nabla f(x))$
    repeat
      $t \leftarrow \beta t$
      $f_{lin} \leftarrow f(x) - \alpha t||\nabla f(x)||_2^2$
      $f_{new} \leftarrow f(x - t\nabla f(x))$
    until $f_{new} \leq f_{lin}$
    $x \leftarrow x - t\nabla f(x)$
  until convergence

4 Experiments

In all experiments, we use stack-of-spirals trajectory to sample k-space, since it efficiently utilizes hardware and allows fast sampling with minimal image-domain distortions. In high resolution experiments, we use variable-density spirals to enable sampling of higher spatial frequencies while preserving scan time and image quality [17]. Spiral trajectories are also well-suited for compressed sensing; performing undersampling by removing a randomly chosen subset of interleaves produces adequately incoherent artifacts. Promising results using this undersampling method have been reported previously [14]. For reconstruction of an image sequence, temporally-incoherent artifacts are desirable. To achieve this, we remove different, randomly chosen subsets of interleaves from each frame.

4.1 Phantom Experiment

To test the reconstruction procedure, a Shepp-Logan phantom image was modified to simulate fMRI dataset. Modified phantom was a sequence of 120 70x70 pixel images, with sinusoidal modulation added to model BOLD signal time course. The period of the sinusoid was 20 frames, and the amplitude ranged from 1% to 5% of the maximum signal value. Region of activation consisted of a 3x3 pixel region in the image (0.17% of total image area). Complex-valued gaussian noise with $\sigma = 5\%$ signal amplitude was added to image-domain data. Apart from the activation pattern described above, all frames were identical. Addition of noise significantly degraded sparsity of the data, but was necessary to produce a reasonable model for fMRI data.

K-space was sampled using a ten-interleaf spiral (via inverse gridding) and undersampling was done by removing randomly chosen interleaves from each frame. Different interleaves were removed from each frame, leading to significant, time-varying aliasing artifacts. Phantom reconstructions were performed from a fraction of available k-space data, ranging from 10% to 90% (corresponding to 1-9 kept interleaves), yielding undersampling factors of 1.1X to 10X (undersampling = total data / available data). To visualize the algorithm's ability to reconstruct the activation sinusoid in correct location, we calculate coherence maps, according to:

$$c = \frac{|f_6|}{\sqrt{\sum_{i=1}^{T/2} |f_i|^2}} \tag{6}$$

Here f is the Fourier transform of the time series of each pixel in the image and f_6 is the paradigm frequency. Informally, equation (6) measures the amount of energy the activation sinusoid contributes to the voxel time series.

Figure 1 summarizes results of the phantom experiment. For the adverse, high noise ($\sigma = 5\%$), low signal amplitude (1%) condition that was tested, signal was well reconstructed from 50 % and even 30 % data: activated region was correctly localized (Figure 1a), and the time series remained close to the truth (Figure 1b). Higher undersampling factors caused

distortions in time series and ambiguous coherence maps. For all signal amplitudes (1%, 3%, 5%), coherence in the region of interest (ROI) for reconstructions from as little as 40% data reached or exceeded corresponding ground truth value (Figure 1c). Sampling patterns used in reconstructions, which highlight random temporal sampling, are shown in Figure 1d. In each column, white and black pixels indicate interleaves that were and were not acquired, respectively.

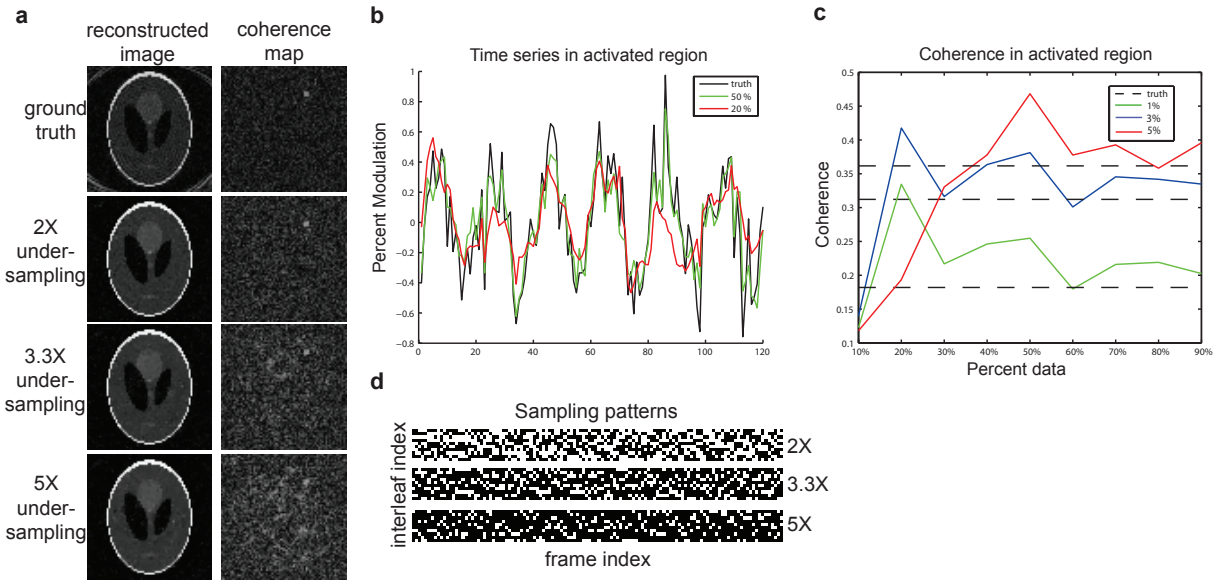

Figure 1: fMRI phantom experiment. **a**, reconstructed images and coherence map for several undersampling factors. **b**, reconstructed time series in the "activated" region. **c**, coherence in the ROI for different signal amplitudes and undersampling factors. **d**, sampling patterns used in the reconstruction

4.2 Undersampled fMRI experiment

To verify the algorithm's ability to accurately reconstruct activation maps and signal dynamics in real data, previously acquired ofMRI dataset was used. Data was acquired on Bruker 7T small bore scanner with 39.6 G/cm maximum gradient amplitude and 457 G/cm/s maximum slew rate.

While gradient recalled echo fMRI sequences are more commonly used, imaging based on balanced steady state free precession (SSFP) makes it possible to acquire 3D volume with improved SNR, reduced image distortions and signal dropout [18; 19]. These properties are desirable for compressed sensing, since 3D Fourier encoding provides large flexibility in choice of sampling trajectory and undersampling pattern, while decrease in noise improves signal sparsity. We thus tested the algorithm on fMRI dataset acquired with 3D pass-band balanced SSFP sequence. Pulse sequence was a 10 interleave stack-of-spirals with 32 k_z encodes, 35x35x16 mm^3 field of view, 500x500x500 um^3 resolution, and 70x70x32 matrix size. Repetition time was 9.375 ms, echo time was 2 ms, and scan time – 3 seconds. Disregarding dummy scans needed to bring magnetization into steady state, functional experiment consisted of 130 scans (390 seconds). First 30 s were used to estimate functional baseline and were followed by 6 cycles of 20 s stimulation and 40 s rest.

Undersampling was performed by removing a randomly chosen subset of all interleaves from available data. As in the phantom experiment, different interleaves were removed in each frame. Since for a general object energy concentration of k-space can be assumed to be approximately spherical, undersampling density along phase encode axis (k_z) was variable, decreasing toward high k_z values. Reconstructions were performed on datasets undersampled by 1.5X, 2X, and 3X. Since bSSFP images exhibit off-resonance banding artifacts, two datasets per undersampling factor (acquired with 0° and 180° phase) were reconstructed and combined by maximum intensity projection (MIP). Figure 2 displays coherence maps, calculated according to $c = \frac{|f_6|}{\sqrt{\sum_{i=1}^{T/2} |f_i|^2}}$, phase maps calculated as $\phi = \angle f_6$, and BOLD response time series. All images are thresholded at $c = 0.35$. To make the time series comparison fair, the same voxels were considered in reconstructed datasets, using the ROI selected from the ground truth dataset. Response time series from the reconstructed (green) and fully sampled (black) data are shown on the same plot to facilitate comparison. Evidently, in datasets reconstructed from 66% and 50% data, activated region is correctly localized and time series of the response closely follows the ground truth. In dataset reconstructed from

33% data, response is distorted and activation maps are significantly noisier. Increase in number of activated pixels in highly undersampled data can be understood by considering minimization of $||D_4 x||_1$ as application of a nonlinear low-pass filter. Minimization of ℓ_1 norm of pixelwise difference between consecutive images removes some high frequency oscillations in time series, decreasing $\sqrt{\sum_{i=1}^{T/2} |f_i|^2}$ and effectively increasing coherence coefficient.

4.3 High Resolution fMRI

Previous applications of compressed sensing MRI sought to reduce imaging time or improve temporal resolution by reducing the number of acquired k-space samples. Instead, we trade off the possible reduction in scan time to attain higher spatial resolution in 3D bSSFP fMRI experiments. To do so, we designed a pulse sequence with sampling trajectory extending farther in k-space, allowing sampling of high spatial frequencies, while overall resulting in sparsely sampled k-space, as illustrated in Figure 3. To demonstrate that this small modification to the acquisition protocol can yield improvements in spatial resolution, we compared results with ones acquired using the standard pulse sequence. Except for the difference in spatial resolution, both sequences had the same relevant imaging parameters: TR = 9.375 ms, TE = 2 ms, FOV = 35x35x16 mm^3, 32 slices/k_z encodes, readout duration = 1.7 ms, flip angle = 30°, total imaging time = 3 s. To attain maximum gain in spatial resolution while preserving short readout duration, variable density sampling was employed in high resolution sequence.

Results are demonstrated on two datasets, with resolution 320×320×500 um^3 and 210×210×500 um^3, and matrix sizes 110×110×32 and 167×167×32. Each CS-reconstructed dataset is compared to corresponding low-resolution fully sampled dataset, acquired during the same imaging session. Trajectories for the CS pulse sequence were designed for 20 and 30 interleaves, requiring 640 and 960 TRs (alternatively: 6 and 9 seconds of imaging time) to acquire full data. To keep total imaging time at 3 s, only 320 TRs were performed per scan, by acquiring a subset of all interleaves. This yields 2X and 3X undersampling

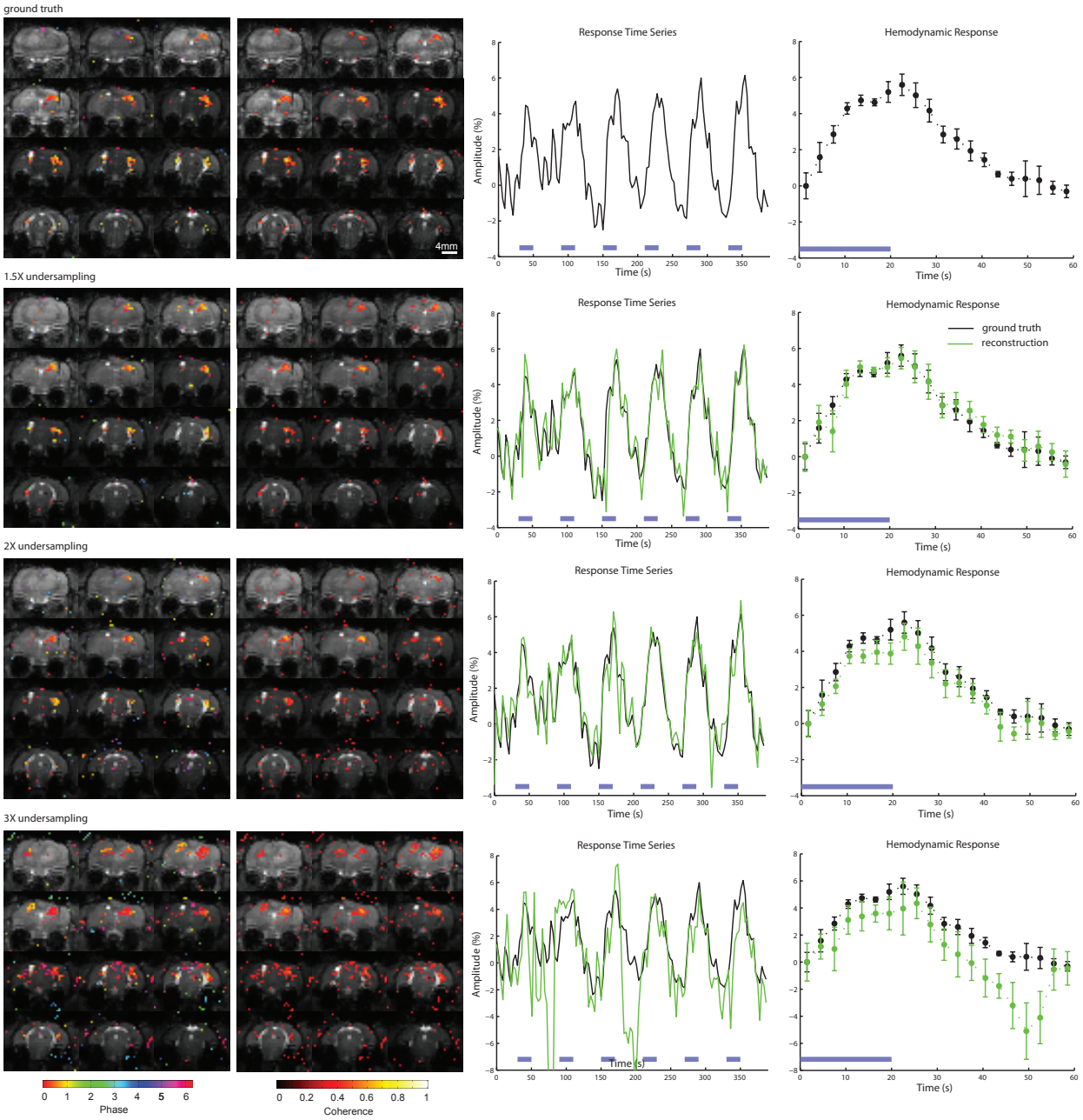

Figure 2: Undersampled fMRI data. Feasibility of reconstructing activation maps and BOLD signal dynamics from a fraction (66%,50%,33%) of total data is verified on a bSSFP dataset.

factors, meaning that two and three times more data would need to be acquired to support given resolution. These undersampling factors result in substantial increase in number of encoded voxels in image domain; matrix sizes increase by factors of $(110/70)^2 = 2.4$ and $(167/70)^2 = 5.7$.

Figure 4 compares fully sampled 500×500×500 um^3 acquisition and 320×320×500 um^3 CS-acquisition (2X undersampling). As before, time series from the reconstructed (green) and fully sampled (black) data are shown on the same plot to illustrate close agreement between the two acquisition schemes. Noise in the activation maps (both shown at threshold c=0.35) is not substantially increased, and most regions active in low-resolution data are also active in high-resolution reconstruction. In particular, active volume in fully sampled data is 16.25 mm^3 and it is 12.9 mm^3 in CS-reconstruction. This result indicates possibility of using compressed sensing to achieve more than two-fold increase in image matrix size, without sacrificing any imaging parameters, and with little SNR penalty.

To further test the method, 3X undersampled dataset with 210×210×500 um^3 resolution was acquired and reconstructed, with results shown in Figure 5. In this case, reconstructed activation map with coherence threshold set at c=0.35 reveals significant noise. Instead, considering the above-mentioned nonlinear filtering of time series that results in overall increase of coherence values, c=0.45 was chosen as the threshold for CS-reconstructed data that is equivalent to c=0.35 for fully sampled data. All following operations, e.g. ROI choice, volume calculations, etc. were based on c=0.45 threshold. Active volume in fully sampled dataset is 55.63 mm^3 in cortex region, and 12.25 mm^3 in thalamus. In CS-reconstruction, it is 20.73 mm^3 in cortex and 1.74 mm^3 in thalamus.

5 Discussion

This work demonstrated a method for substantially improving spatial resolution in fMRI experiments by utilizing compressed sensing framework. Feasibility of reconstructing fMRI

data from undersampled kspace was verified on simulated phantom, as well as real fMRI dataset. Results of the proposed high resolution fMRI scheme were demonstrated on two datasets, with over two-fold and five-fold increases in image matrix size, and corresponding increases in spatial resolution. In testing the method, we found that very high undersampling factors (e.g. 3X) result in SNR loss, ultimately resulting in substantial loss of active volume in reconstructions. Despite that, gain in spatial resolution reveals details not seen in fully sampled, low resolution data: for instance, in Figure 5, robust activation of upper cortical layers is much more evident in compressed-sensing reconstruction. Also, acquiring and averaging several scans (which was not done here) can be used to efficiently reduce noise. Therefore, improving spatial resolution using this method can make it possible to extend conclusions drawn from fMRI data and facilitate its interpretation.

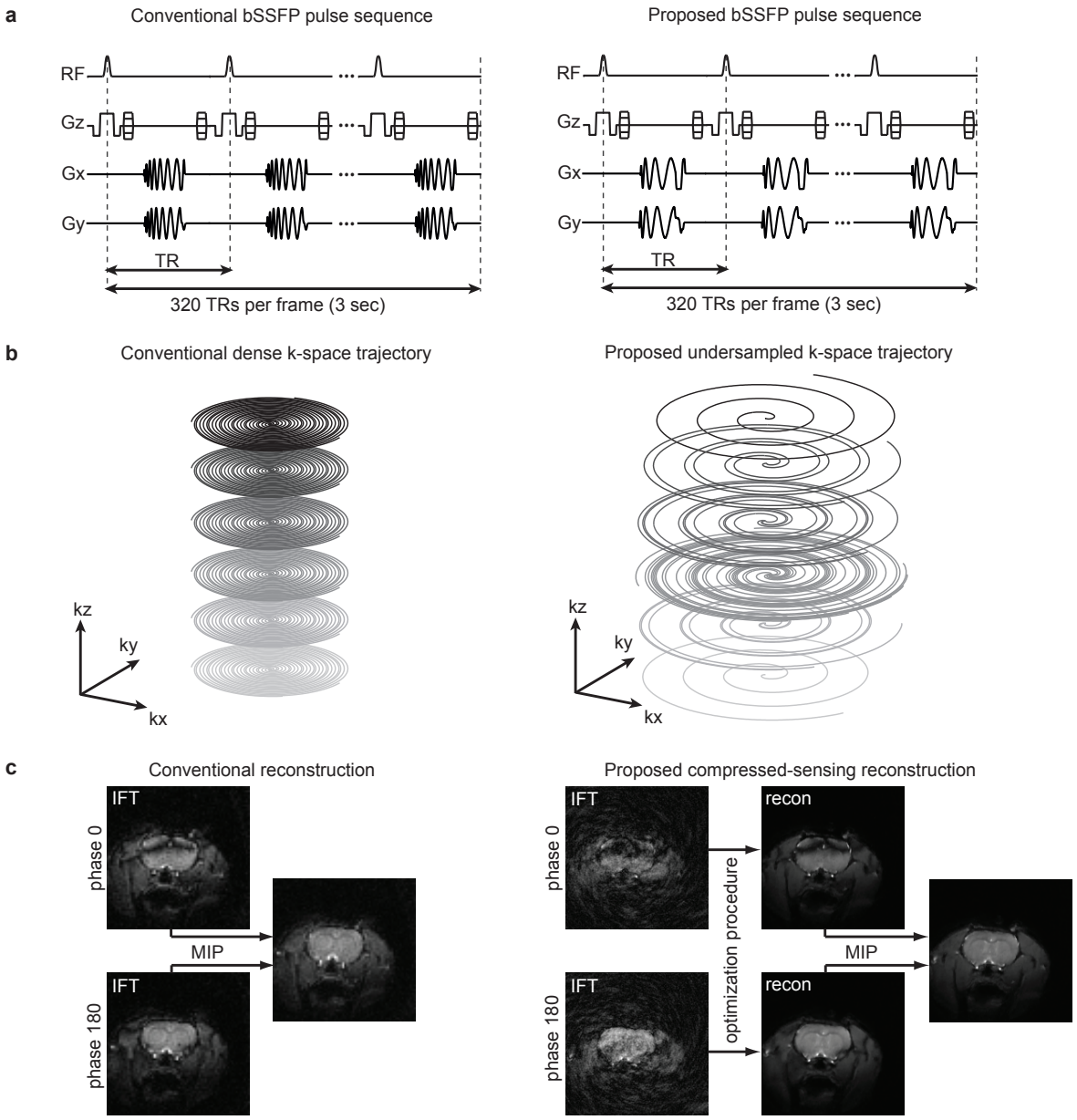

Figure 3: Overview of proposed high resolution fMRI method. **a**, pulse sequences for the two methods differ only in gradient waveforms; relevant imaging parameters remain the same. **b**, conventional trajectory results in dense sampling near k-space origin, due to sampling at Nyquist rate. Proposed trajectory allows sampling of high spatial frequencies by extending further from k-space origin, but overall results in sparse sampling below Nyquist rate. **c**, conventional reconstruction only requires inverse Fourier transform (IFT) and MIP combination. Proposed method requires solving optimization problem (5) to suppress aliasing artifacts, before MIP can be applied.

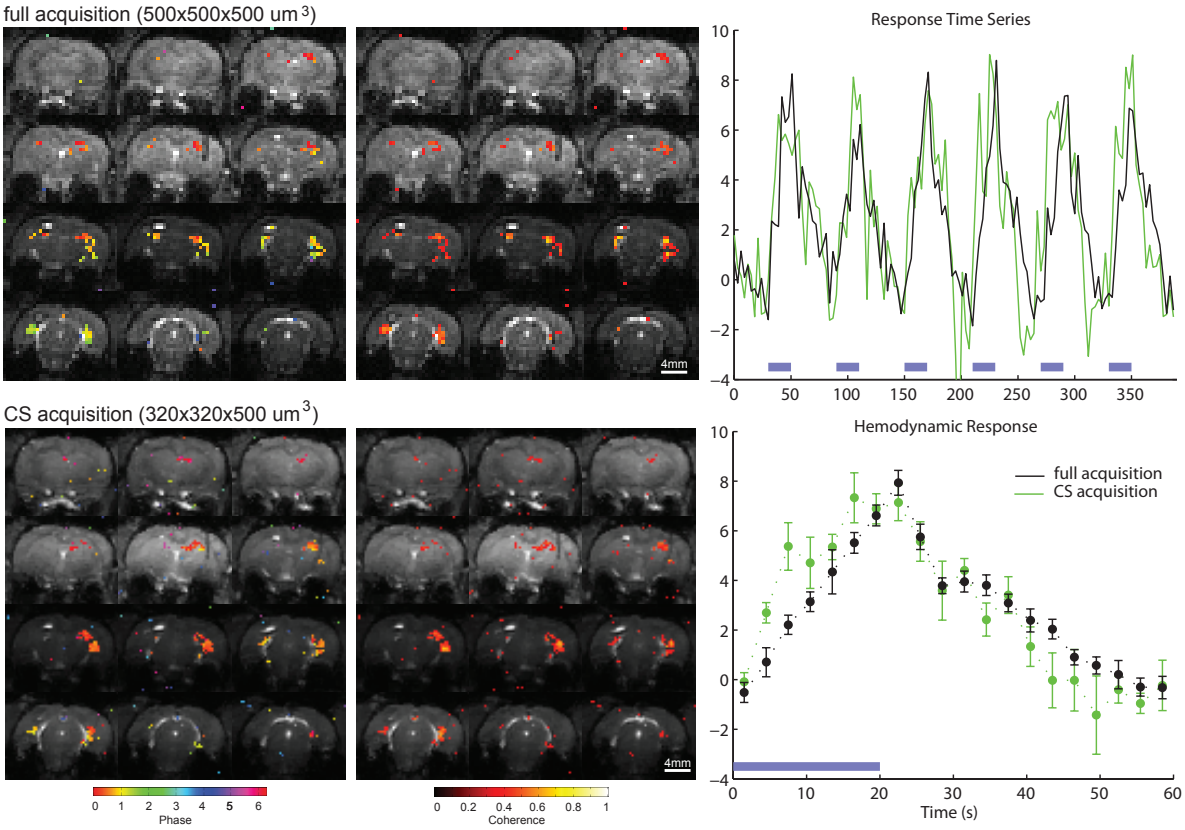

Figure 4: High resolution fMRI: reconstruction from 2X undersampled data.

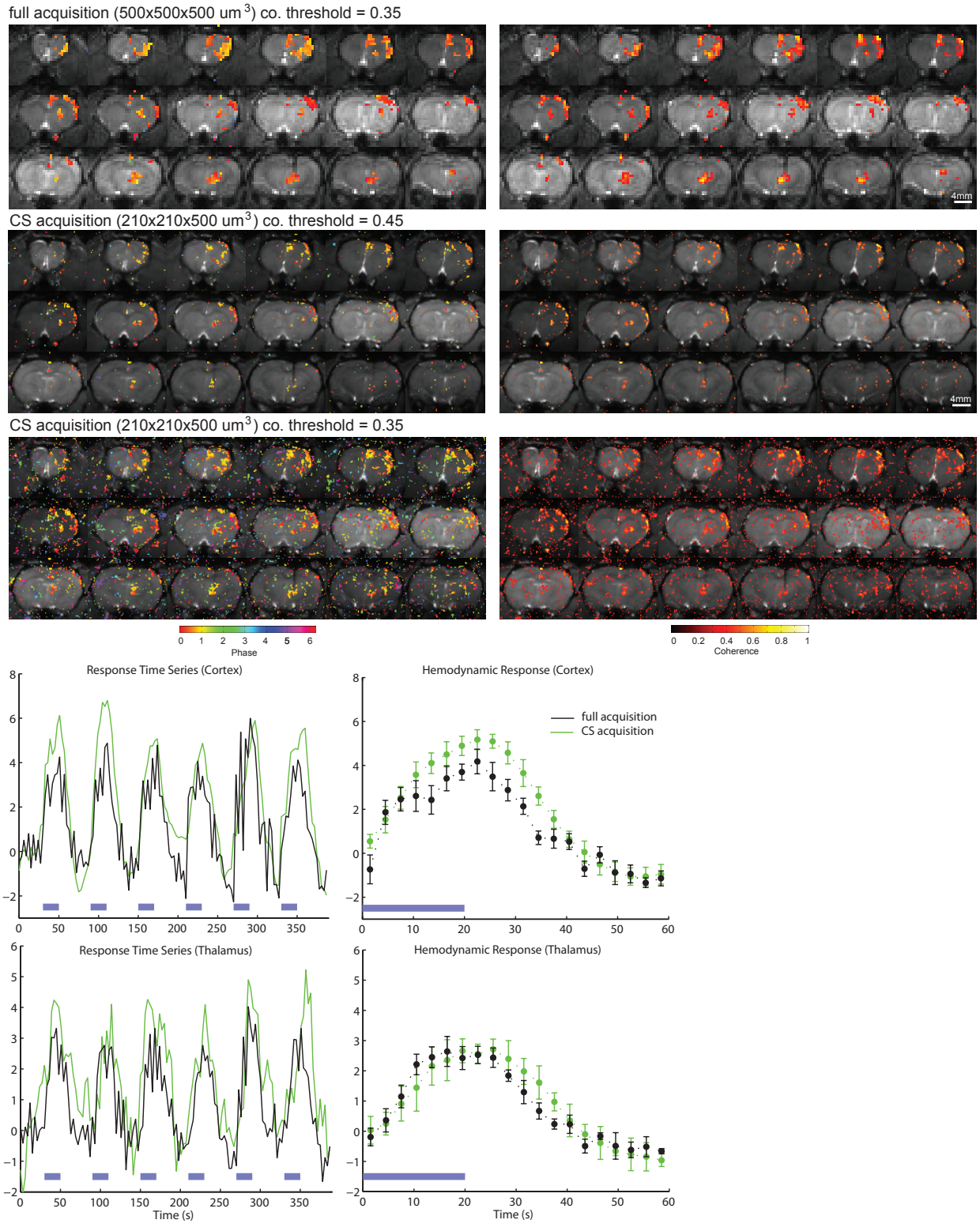

Figure 5: High resolution fMRI: reconstruction from 3X undersampled data.

Bibliography

[1] S. Ogawa, T. M. Lee, A. R. Kay, and D. W. Tank, "Brain magnetic resonance imaging with contrast dependent on blood oxygenation," *Proceedings of The National Academy of Sciences*, vol. 87, pp. 9868–9872, 1990.

[2] E. J. Candes, J. K. Romberg, and T. Tao, "Robust uncertainty principles: exact signal reconstruction from highly incomplete frequency information," *IEEE Transactions on Information Theory*, vol. 52, pp. 489–509, 2006.

[3] D. L. Donoho, "Compressed sensing," *IEEE Transactions on Information Theory*, vol. 52, pp. 1289–1306, 2006.

[4] J. H. Lee, R. Durand, V. Gradinaru, F. Zhan, I. Goshen, D.-S. Kim, C. Ramakrishnan, L. E. Fenno, and K. Deisseroth, "Global and local fMRI signals driven by neurons defined optogenetically by type and wiring," *Nature*, vol. 10, no. 465, pp. 788–792, 2010.

[5] E. Candes and J. Romberg, "Sparsity and incoherence in compressive sampling," *Inverse Problems*, vol. 23, no. 3, pp. 969–985, 2007.

[6] M. Lustig, D. Donoho, and J. M. Pauly, "Sparse MRI: The application of compressed sensing for rapid MR imaging," *Magnetic Resonance in Medicine*, vol. 58, pp. 1182–1195, 2007.

[7] S. Ajraoui, K. J. Lee, M. H. Deppe, S. R. Parnell, J. Parra-Robles, and J. M. Wild, "Compressed sensing in hyperpolarized He-3 lung MRI," *Magnetic Resonance in Medicine*, vol. 63, pp. 1059–1069, 2010.

[8] Y.-C. Kim, S. S. Narayanan, and K. S. Nayak, "Accelerated three-dimensional upper airway MRI using compressed sensing," *Magnetic Resonance in Medicine*, vol. 61, pp. 1434–1440, 2009.

[9] M. Lustig, J. Santos, D. L. Donoho, and J. M. Pauly, "k-t SPARSE : High frame rate dynamic MRI exploiting spatio-temporal sparsity," vol. 50, p. 2420, 2006.

[10] U. Gamper, P. Boesiger, and S. Kozerke, "Compressed sensing in dynamic MRI," *Magnetic Resonance in Medicine*, vol. 59, pp. 365–373, 2008.

[11] H. Jung, K. Sung, K. S. Nayak, E. Y. Kim, and J. C. Ye, "k-t FOCUSS: A general compressed sensing framework for high resolution dynamic MRI," *Magnetic Resonance in Medicine*, vol. 61, pp. 103–116, 2009.

[12] H. Jung and J. C. Ye, "Performance evaluation of accelerated functional MRI acquisition using compressed sensing," in *Proceedings of the Sixth IEEE International Conference on Symposium on Biomedical Imaging*, pp. 702–705, 2009.

[13] L. I. Rudin, S. Osher, and E. Fatemi, "Nonlinear total variation based noise removal algorithms," in *International Symposium on Physical Design*, 1992.

[14] M. Lustig, J. H. Lee, D. L. Donoho, and J. M. Pauly, "Faster imaging with randomly perturbed, undersampled spirals and ℓ_1 reconstruction," in *Proceedings of the ISMRM Annual Meeting (ISMRM'05)*, p. 685, 2005.

[15] T. Chang, L. He, and T. Fang, "MR image reconstruction from sparse radial samples using bregman iteration," in *Proceedings of the ISMRM Annual Meeting (ISMRM'05)*, p. 696, 2005.

[16] J. A. Fessler and B. P. Sutton, "Nonuniform fast fourier transforms using min-max interpolation," *IEEE Transactions on Signal Processing*, vol. 51, pp. 560–574, 2003.

[17] J. H. Lee, B. A. Hargreaves, B. S. Hu, and D. G. Nishimura, "Fast 3D imaging using variable-density spiral trajectories with applications to limb perfusion," *Magnetic Resonance in Medicine*, vol. 50, pp. 1276–1285, 2003.

[18] J. H. Lee, S. O. Dumoulin, E. U. Saritas, G. H. Clover, B. A. Wandell, D. G. Nishimura, and J. M. Pauly, "Full-brain coverage and high-resolution imaging capabilities of passband b-SSFP fMRI at 3T," *Magnetic Resonance in Medicine*, vol. 59, pp. 1099–1110, 2008.

[19] K. L. Miller, S. M. Smith, P. Jezzard, and J. M. Pauly, "High-resolution fMRI at 1.5T using balanced SSFP," *Magnetic Resonance in Medicine*, vol. 55, pp. 161–170, 2006.